Structural Evidence for the Ordered Crystallites of Ionic Liquid in Confined Carbon Nanotubes

Kun Dong, Guohui Zhou, Xiaomin Liu, Xiaoqian Yao, and Suojiang Zhang*

State Key Laboratory of Multiphase Complex Systems, Institute of Process Engineering, Chinese Academy of Sciences, 100190 Beijing, China

Alexander Lyubartsev

Division of Physical Chemistry, Arrhenius Laboratory, Stockholm University, S10691 Stockholm, Sweden

Received: January 19, 2009; Revised Manuscript Received: April 15, 2009

Ionic liquids (ILs) are a class of new green materials that have attracted extensive attention in recent decades. Many novel properties not evident under normal conditions may appear when ionic liquids are confined to a nanometer scale. As was observed in the experiment, an anomalous phase behavior from liquid to high melting point perfect crystal occurred when 1-*n*-butyl-3-methylimidazolium hexafluorophosphate ([bmim][PF_6]) ionic liquid was confined in a carbon nanotube. In this work, we performed molecular dynamics (MD) simulations for [bmim][PF_6] ionic liquid and provided direct structural evidence that the ionic crystallizes in a carbon nanotube. The ordered ionic arrangement in both the radial and the axial directions can be observed inside the channels of the CNTs to induce the form of crystallites. The ionic stacking and distributing can be determined by the sizes of the CNTs. Hydrogen bonds remain the dominant interactions between cations and anions when the ionic liquid enters into the CNT from the bulk phase. The free energies as the thermal driven forces were calculated, and it is found that it is very difficult for a single anion to enter into the channel of the CNT spontaneously. A more favorable way is through an ion-pair in which a cation "pulls" an anion to enter into the channel of the CNT together. It is predicted that other ionic liquids that possess similar structures, even including the pyridinium-based ionic liquids, can show higher melting points when confined in CNTs.

1. Introduction

Room-temperature ionic liquids (RTILs) have been gaining widespread attention in industries and academia due to their special properties,[1,2] which are determined by their unique structures as inherent driving forces. The main difference between RTILs and simple molten salts is that the RTILs are composed of bulky, asymmetrical ions that can only loosely fit together so that they can form only the liquid state at room temperature. In recent years, the vast experimental and theoretical investigations have focused on RTILs.[3−8] Theoretical calculations, including quantum chemistry (QM) and classical molecular dynamics (MD) simulations, have been performed to explore the structures of the various RTILs.[4−6] Many of the researches have indicated that the hydrogen bonds are the main interactions between cations and anions in the bulk phase. As one of the most studied RTILs, [bmim][PF_6] has been used as a prototype in many processes,[1,2,9,10] and a number of computations have also been performed to understand the intermolecular structure and dynamics of this compound.[11−15] Our recent works[11] explored the interactions of [Dmim][PF_6] ionic liquid in bulk phase using the ab initio method, and it was found that there were more than two hydrogen bonds in each ion-pair, and a hydrogen-bonded network might be formed by the connection of these hydrogen bonds. Morrow et al.[15] carried out the MD simulations for [bmim][PF_6] in the isothermal−isobaric ensemble, and the results indicated that anions tend to orient near the C(2) atoms of imidazolium rings of cations and more than one hydrogen bond can be formed between these C−H groups of cations and F atoms of anions.

However, as many experiments have proved, ionic liquid being confined in nanometer scale can be induced to demonstrate many novel phenomena, especially the anomalous phase behavior and the form of crystallites, which are very different with the bulk phase. Liu et al.[16] observed the coexistence of liquid and solid phases and the forms of nanometer droplets when [bmim][PF_6] was coated on the surface of mica at room temperature. When mixed with imidazolium-based ionic liquid, the heavily entangled nanotube bundles formed gels after being ground and changed into the much finer bundles. The phase transition suggests that these gels are formed by physical cross-linking of the nanotube bundles, mediated by local molecular ordering of the ionic liquids.[17] A more conspicuous phase transition was observed when [bmim][PF_6] was filled into the carbon nanotube (CNT), a type of desirable nanometer material that provided the promising candidates as building blocks for nanometer scale environment. The melting point of [bmim][PF_6] was increased largely, from −6 to above 200 °C, providing possibility for obtaining a better crystal.[18]

As known, molecules can be encapsulated to form quasi-1D arrays in CNTs. Many substances, including water, organic and inorganic solvent, gas, and inorganic ions have been introduced into the channels of CNTs.[19] The transporting and stacking of these substances in CNTs are of great interest both theoretically and practically for various applications.[20−26] Significant phase transition for water from liquid to solid has been proven by

* Corresponding author. Phone/fax: 01-86-82627080. E-mail: sjzhang@home.ipe.ac.cn.

10.1021/jp900533k CCC: $40.75
Published on Web 05/13/2009

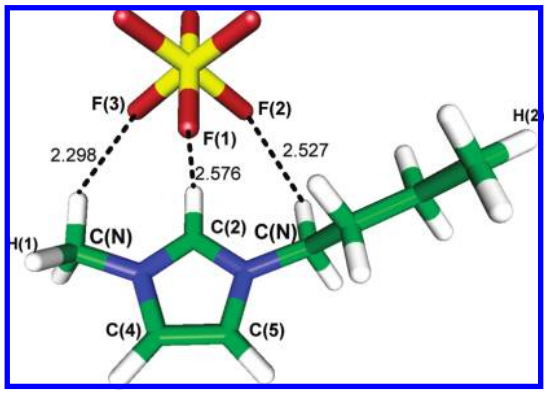

Figure 1. The optimized ion-pair structure of [bmim][PF_6] at B3LYP/6-31+G* level of DFT theory. N atoms are blue, C atoms are green, F atoms are brown, and P atoms are yellow, the C(2), C(4), and C(5) atoms locate on the imidazolium plane, the C(N) atoms connect with the N atoms in side chains. The three shortest distances (F(1)···H, F(2)···H, and F(3)···H) between cation and anion were 2.576, 2.527, and 2.298 Å, respectively.

many experiments and theoretical calculations when water is confined in nanotubes,[27−30] and ring-stacked *n*-gonal structures have been found in single-wall CNTs.[31−33] In the past decade, many inorganic ionic compounds, including the KI, NiS_2, Ws_2, etc., have been filled into the carbon nanotubes where they were shown to form low-dimensional ordered (crystalline) structures,[34−38] which demonstrated that some traditional views of phase behaviors for even simple elements required reevaluation. The form of crystallites and the significant solid phase property of ILs in nanometer scale may bring new opportunities for many future applications, which are difficult to obtain in traditional conditions due to the existence of the glass state. As compared to these inorganic compounds, ionic liquids possess a lower melting point, higher viscosity, and worse fluidity.[34,39,40] However, up-to-date, there was little understanding about molecular stacking, hydrogen bonds, and confined structures for the crystallites of ionic liquid confined in carbon nanotubes, which limits the further exploitation for the new material seriously. Therefore, to get insight into the structural and phase behavior properties of IL confined in CNT, we performed in this work molecular dynamics simulations with the purpose to investigate the ionic distribution, hydrogen bonds, and the thermodynamically driven forces for [bmim][PF_6] in different diameters single-wall carbon nanotubes.

2. Methodology and Simulation Details

2.1. Initial Configuration Setup. The density functional theory (DFT) was used to study the single ion-pair structure. Figure 1 shows an optimized ion-pair structure of [bmim][PF_6] at B3LYP/6-31+G* level. The anion localizes above the imidazolium ring of the cation, and the distance between the H(1) atom and H(2) atom is 9.89 Å, which is the longest radial distance of the ion-pair. Considering the size and flexibility of the $[bmim]^+$ cation, we chose two different diameter rigid single-wall CNTs, (9, 9) CNT and (10, 10) CNT, in which all of the carbon atoms are sp^2 hybrid, and each could contain a single ion in the radial direction. Table 1 gives the number of carbon atoms, diameters (*D*), and lengths (*L*) for the two CNTs. The initial calculated configurations were constructed by removing a cylindrical section from an equilibrated periodic reservoir box that contains 256 $[bmim]^+$ cations and 256 $[PF_6]^-$ anions, and then introducing a CNT with required size. Both ends of the CNT were temporarily sealed with a pair of end-plates to allow

TABLE 1: Simulation Cases for Carbon Nanotubes, Where (*m*, *n*) Are the Carbon Nanotube's Indices, *D* Is the Carbon Nanotube's Diameter, and *L* Is the Carbon Nanotube's Length

carbon nanotube (*m*, *n*)	(9, 9)	(10, 10)
carbon atoms	432	480
D/Å	12.20	13.56
L/Å	29.51	29.51

the system to be pre-equilibrated. Without any initial filling, the MD simulations were performed with cutoff of large forces and temperature scaling at each time step to remove possible atomic overlapping during 5000 MD steps. After the pre-equilibration was finished, the end-plates were removed, and the IL was allowed to fill into the tube from the bulk outer liquid. Figure 2 shows the initial configuration for the simulations. The filing processes were typically completed after about 1.0 ns time, in Nose−Hoover[41] NpT ensemble with coupling constants of 700 and 80 fs to the pressure and temperature bath, respectively, during which the system density gradually increased to the experimental value (1.23−1.36 g/cm^3).

2.2. Simulation Method Details. In the MD simulations, the Amber all-atoms force field was applied. For the CNTs, only the Lennard-Jones (LJ) potential was taken into account, and the parameters for ε and σ were set up to 0.36 kcal/mol and 0.40 nm.[42] The force field parameters of $[bmim]^+$ cations and $[PF_6]^-$ anions were adopted from Liu's work.[43] The total interaction potential between IL and the carbon atoms of CNT was calculated by the site−site interaction method with the following form:

$$U_{IC} = 4\varepsilon_{IC}\sum_{i=1}^{N_I}\sum_{j=1}^{N_C}\left[\left(\frac{\sigma_{IC}}{r_{ij}}\right)^{12} - \left(\frac{\sigma_{IC}}{r_{ij}}\right)^{6}\right] \quad (1)$$

where the cross-correlation LJ parameters σ_{IC} and ε_{IC} were determined by the Lorentz−Berthelot rules.

MD simulations were performed using M.Dynamix 5.2[44] with the temperature and the pressure being 500 K and 1.0 bar, respectively. Periodic boundary conditions were applied with Ewald summation of the electrostatic interactions for the ionic liquid. The Tuckerman−Berne double time step algorithm[45] was employed with 2 and 0.2 fs time steps, respectively. The short time step was used for integrating intramolecular vibrations and nonbonded interactions within 5 Å distance, while the larger time step was used for integrating LJ and electrostatic forces within 15 Å cutoff distance.

2.3. Expanded Ensemble Method. The molecular dynamics-expanded ensembles (EE) method[46,47] has been previously used

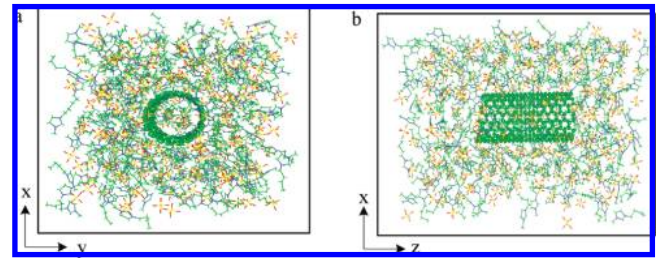

Figure 2. The initial simulation configurations in the periodic reservoir box. (a) Lateral view; (b) side view. The CNT was placed in the center of the reservoir box along the *z*-axis and drawn in a stick−ball representation. The surrounding ionic liquid was drawn in wireframe representation.

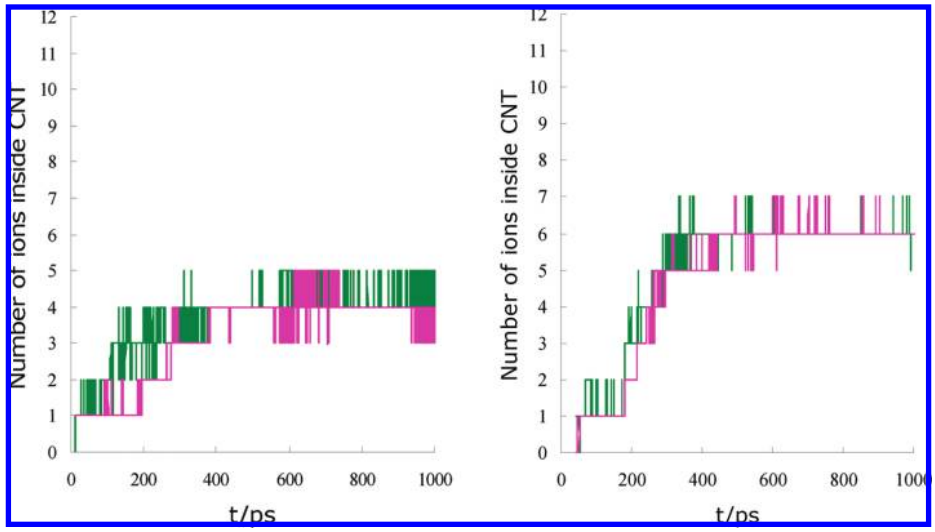

Figure 3. The filling processes of ionic liquid in CNT (9, 9) and CNT (10, 10). The green represents the filling number of cations, and the pink represents the filling number of anions.

to calculate the solvation free energies for the large molecules or the polymer solution in previous reports.[48] The method is now implemented as a part of the M.Dynamix 5.2 package.[44] The general idea of the EE method is based on Monte Carlo transitions between the canonical ensembles defined by the configuration partition function:

$$Z = \sum_{m=0}^{M} Z_m \exp(\eta_m) = \sum_{m=0}^{M} \int_V \prod_i^{N+1} \mathrm{d}q_i \exp\{-\beta[H_N(q_i) + H_{\mathrm{int}}(q_{N+1}) + h_{N+1}(\alpha_m, q_i)] + \eta_m\} \quad (2)$$

where $\beta = 1/kT$, H_N is the potential energy of N solvent particles having coordinates q_i, H_{int} is the intramolecular potential energy of the solute, h_{N+1} is the potential energy of interaction of $N+1$th (solute) particle with all other solvent particles, α_m is the particle insertion parameter changing from 0 to 1 while m changes from 0 to M, and η_m's are the balancing factors, which are introduced to facilitate changes of the insertion. The solute−solvent interaction energy $h_{N+1}(\alpha_m,q_i)$ is equal to 0 at $\alpha_0 = 0$ and is equal to the true solute−solvent interaction (determined by the force field) at $\alpha_M = 1$, gradually changing with α between the extreme cases. In case of computing excess free energy of several molecules simultaneously (for example, for an ion-pair), the potential $h(\alpha_m,q_i)$ includes also intermolecular interaction between different inserted molecules. A Monte Carlo random walk in the expanded space of $\{q_i\}$ and m, consisting of displacements of both particles and changes of m, produces a probability distribution over the subensembles p_m. In the molecular dynamics formulation of EE, motion in the "true" coordinate space $\{q_i\}$ is performed by molecular dynamics, while transitions between subensembles are still made by the Metropolis Monte Carlo rules. The excess (Helmholtz) free energy can be determined from the probability ratio of the two extreme subensembles:

$$\beta\Delta F = -\ln \frac{P_M}{P_0} + \eta_m - \eta_0 \quad (3)$$

The simulation is carried out in the NPT ensemble, and eq 3 defines the Gibbs free energy difference.

In previous works on the expanded ensembles, a linear dependence of h on α was typically used.[44,46−48] It was argued that this may be not efficient for large molecules because effective LJ size of the particle changes very slowly with α, and some other couplings of the solute−solvent interaction were considered.[49] In the present work, we used the following procedure of scaling the solute−solvent interaction with α: the electrostatic energy is scaled as α^2, the ε parameter scales linearly with α, while σ parameter scales as $\alpha^{1/3}$ (the last condition corresponds to a linear scaling of the effective particle volume with α). Such scheme has allowed us to make repeated insertion/deletions for rather large molecules during several nanoseconds time with reliable determination of the probabilities in eq 3.

3. Results and Discussion

3.1. Filling and Distribution of Ionic Liquid in CNTs. Despite its hydrophobic character, the initially empty channel of CNT can be spontaneously filled by surrounding liquid in the reservoir and reached a saturated state in the period of 1.0 ns. Figure 3 shows the filling processes in both (9, 9) and (10, 10) CNTs. In the end, there are 4 cations and 4 anions to enter into the channel of (9, 9) CNT. In the (10, 10) CNT case, the numbers of both cations and anions are 6, respectively. Although the resulting numbers of cations and anions are the same in both CNTs, it can be seen that the entering speeds of cations are always faster than those of anions. For example, the shortest entering time is 300 ps for cation and 600 ps for anion when the ionic number is 4 in (9, 9) CNT. The shortest entering time is 360 ps for cation and 450 ps for anion when the ionic number is 6 in (10, 10) CNT, respectively (as shown in Figure 3). Generally, the cations are always faster than the anions in the whole filling process. Comparing both CNTs, it can be found that the larger diameter CNT can accommodate more ions and provide faster filling speed for the same entering ionic number.

3.2. Radial Distributions of Ions in CNTs. Nanometer scale confinement has been known to be able to induce heterogeneous density distribution, mainly in the radial direction. When confined in different size CNTs, water molecules are distributed in the corresponding cylindrical sheet and form different stacking shape.[18] As compared to water, the structure of ionic liquid is much more complicated, so to investigate the ionic distribution along the radial direction, in this simulation we selected the

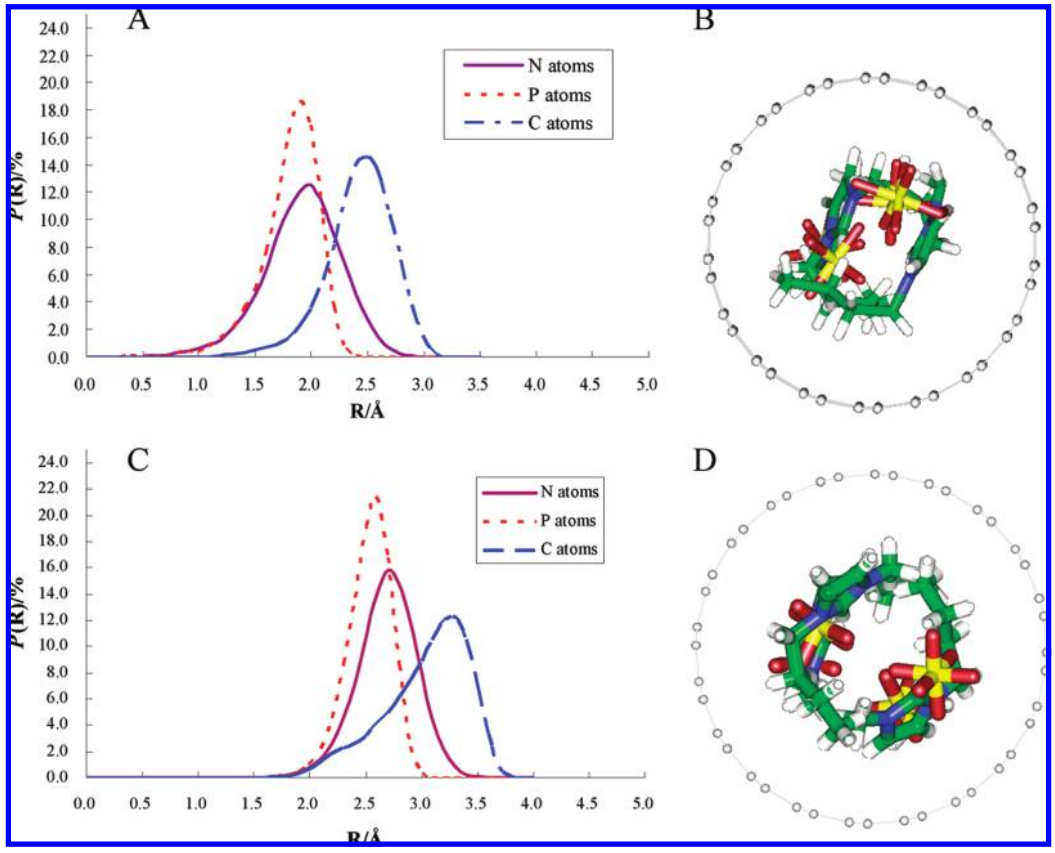

Figure 4. The radial distributions of characteristic atoms (N atoms, C atoms, and P atoms) and the snapshots in CNTs. Parts (A) and (B) show this distribution and a snapshot in (9, 9) CNT. Parts (C) and (D) show this distribution and a snapshot in (10, 10) CNT.

two nitrogen (N) atoms of the cation to represent the distribution of imidazolium plane, the central phosphorus (P) atoms of anions (which is the mass center of anion) to represent the distribution of the anions, and the carbon (C) atoms on two alkyl side chains to represent the side chains. Figure 4 shows the distributions of these characteristic atoms along the radius r. They are plotted against the radius r of the cylindrical sheet (with $\Delta r = 0.1$ Å, Figure 4A and C), and two snapshots are presented in Figure 4B and D to give clear images of such distributions inside the channels of the two CNTs.

In (9, 9) CNT, the peaks of the radial distributions of both the N and the P atoms locate at 2.0 Å, and the peak of C atoms locates at 2.5 Å (see Figure 4A). In (10, 10) CNT, locations of the three peaks for the P, N, and C atoms are at 2.5, 2.8, and 3.0 Å, respectively (see Figure 4C). This indicates that all of the cations and anions stack in the same cylindrical sheet with the thickness being about 0.5−1.0 Å. The average diameter of the sheet increases with the increasing of the CNT diameter, which is very similar to the water distribution in confined CNT. The hydrophobic nature of C atoms of CNT indicates that it is more stable for RTIL to distribute near the center of the channel of CNT than near the walls. The cylindrical sheet size is related to the diameter of the CNT, and it increases with the increasing diameter of CNT. Considering that the cations possess a long side chain, one can imagine that the cations may be bent along the tube wall of the CNT in the sheet. Generally, the stacking of ions and the forming of an ionic sheet in CNT results in the density heterogeneity along the radial direction.

3.3. Axial Distributions of Ions in CNTs. Imidazolium-based cation has a larger molecular size and is more asymmetrical than its anion counterparts. The orientation of imidazolium plane along the central z-axis plays an important role for the entrance of cations into CNT. Figure 5 shows this orientation distribution of the imidazolium plane along the z-axis inside the channels of both (9, 9) CNT and (10, 10) CNT, respectively. The α angle is defined as the dihedral angle between the imidazolium plane of the cation (formed by C(2), C(4), and C(5) atoms in Figure 1) and the lateral plane (in Figure 2). According to Figure 5, the α angles mainly distribute around 90° inside both channels; this indicates that the imidazolium planes of cations are parallel with the vector normal along the z-axis and such ring-orientations can produce a minimum steric hindrance in the z-axis direction when the cations enter into the channel of CNT.

Figure 6A and C shows the distribution of both N and P characteristic atoms that represent the positions of cations and anions along the central z-axis ($\Delta L = 1$ Å) in the axial direction inside and outside the channel of CNT and plotted against the z-coordinate covering length of 60 Å. Two snapshots are presented in Figure 6B and D to give the clear images of such distributions. The peaks of both N and P atoms in (9, 9) CNT are regularly distributed with a 5 Å interval inside the channel (see Figure 6A). This indicates that each cation distributes along the z-axis with 5 Å interval and is followed by an anion, and both the cations and the anions arrange alternately inside the channel, which forms a one-dimensionally ordered pulse-like ionic chain similar to the arrangement of water in CNT. An image of such arrangement is shown in Figure 6B. Yet outside the channel and near the bulk phase, the disordered arrangement is seen from Figure 6A. In (10, 10) CNT, each cation has nearly the same distribution with each anion (see Figure 6C). This can be found from the snapshot of Figure 6D in which each anion moves above imidazolium planes of cations to form ion-pairs as shown in Figure 1, and these ion-pairs arrange alternately

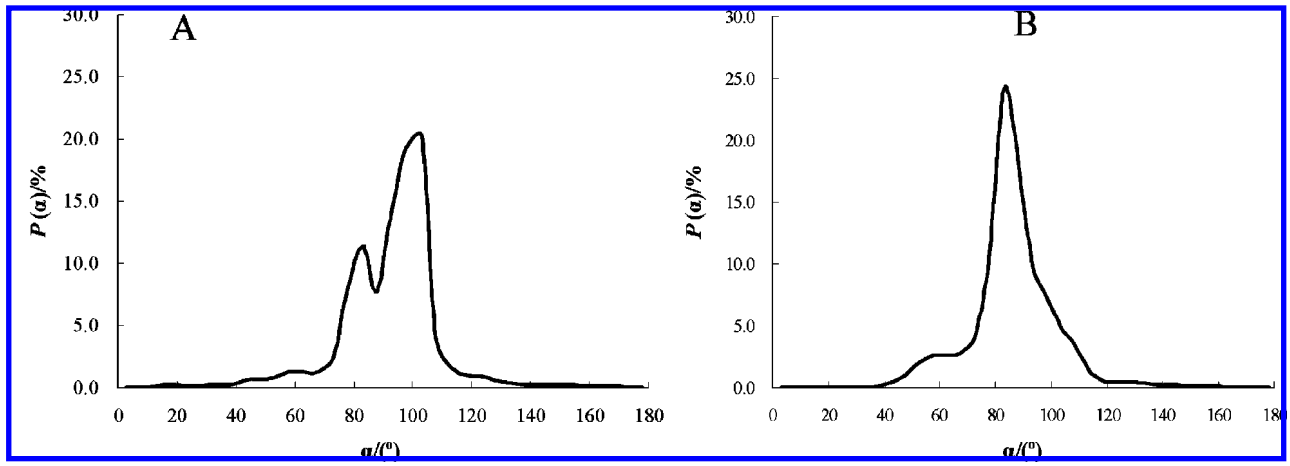

Figure 5. The orientation distribution of imidazolium planes in CNTs. (A) In CNT (9, 9) and (B) in CNT (10, 10). The α angle is defined as the dihedral angle between the imidazolium plane and the lateral plane (see Figure 2).

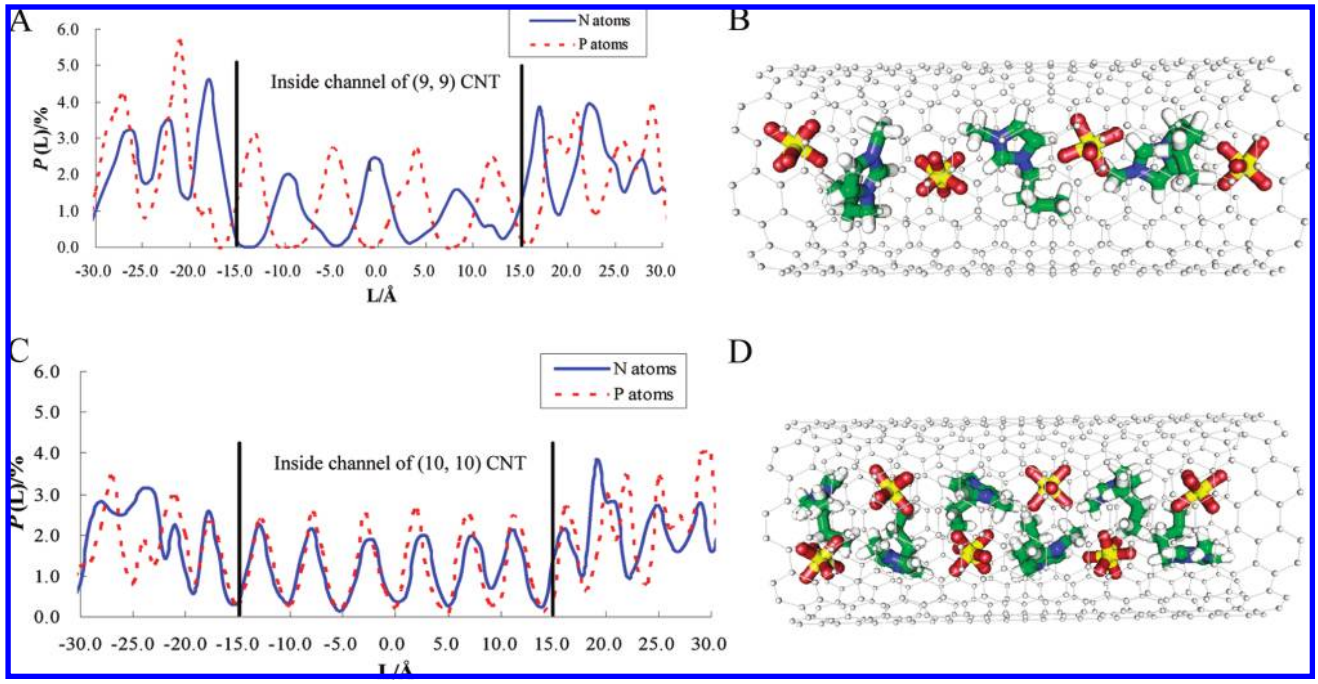

Figure 6. The axial distributions of characteristic atoms (N atoms and P atoms) along the *z*-axis inside channels of the CNTs (*x*-coordinate from −15.0 to 15.0 Å) and outside CNTs (*x*-coordinate from −15.0 to −30.0 Å and from 15.0 to 30.0 Å, respectively) and the snapshots. Parts (A) and (B) show this distribution and a snapshot in CNT (9, 9); parts (C) and (D) show this distribution and a snapshot in CNT (10, 10).

inside the channel with 5 Å interval. Similarly, outside the CNT the ionic arrangement becomes disordered from that inside CNT, which is near the bulk phase distribution.

Many substances confined in CNT may exhibit very different solid−liquid critical points, which cannot occur in the bulk phase. For example, a variety of single-file structures of water inside single-wall CNTs observed by Koga et al.[50] can be rationalized in a phase diagram from liquid to new ice formation. When [bmim][PF_6] was confined inside the channel of the CNT, the ions of disordered arrangement in bulk phase would fill into the CNT and form the ordered arrangement. The structural transformation results in an anomalous phase behavior from liquid to high melting point crystallites, which was also demonstrated by the experimental observation of the anomalous phase transition when [bmim][PF_6] ionic liquid was confined in CNT.[18]

3.4. Hydrogen Bonds of Ionic Liquid in Confined CNTs. Water forms the ring structures in single-wall CNT that involve two types of hydrogen bonds; the hydrogen bonds within the ring structure exhibit frequencies like those found in bulk H_2O, but there is also an unusual stretching frequency of hydrogen bonds formed between neighboring rings. In view of the whole confinement, the hydrogen bonds form a network by the intraring hydrogen bonds and inter-ring hydrogen bonds.[32] Talaty et al.[51] discussed the structures of C_{2-4}mimPF_6 ionic liquids in the bulk phase using DFT methods. They found the hydrogen bonds can be formed between F atoms of anions and C−H groups of cations. We also found the hydrogen-bond network in bulk imidazolium-based ILs in our previous works.[11] Therefore, hydrogen bonds should be the ubiquitous interaction between cations and anions in bulk ionic liquid system due to their special structures and electrostatics. Here, we investigated the distribution and structure of the hydrogen bond when [bmim][PF_6] is confined inside a channel of the CNT. In the DFT optimized structure shown in Figure 1, the shortest distances between cation and anion (F(1)···H, F(2)···H, and F(3)···H) are 2.576, 2.527, and 2.298 Å, respectively. According to the criterion that a hydrogen bond is formed when the

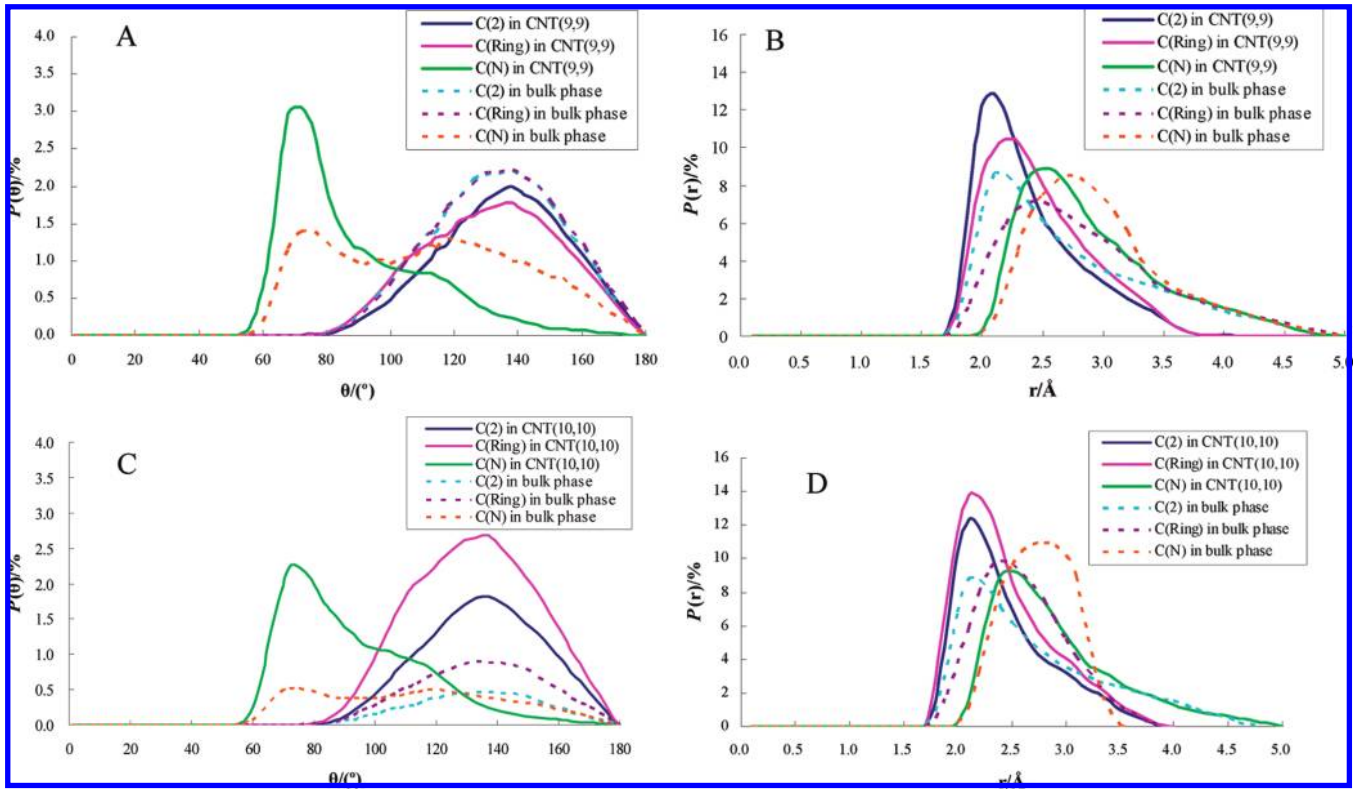

Figure 7. Characteristics of hydrogen bonding between F atoms of anion and H atoms of cations in CNTs and in the bulk phase. (A) The various hydrogen-bond angle distribution in (9, 9) CNT (solid line) and in the bulk phase (dashed line). (B) The distance of F···H distribution in (9, 9) CNT (solid line) and in the bulk phase (dashed line). (C) The various hydrogen-bond angle distribution in (10, 10) CNT (solid line) and in the bulk phase (dashed line). (D) The distance of F···H distribution in (10, 10) CNT (solid line) and in the bulk phase (dashed line). As in Figure 1, C(Ring) includes C(2), C(4), and C(5) atoms on imidazolium ring as noted in Figure 1, and C(N) represents the side chain atoms that connect with N atoms.

distance H···F is shorter than the van der Waals H···F distance of 2.67 Å,[52] it can be deduced that the hydrogen bonds are really formed between the C−H groups of cation and F atoms of anion. Herein, we calculated the angles and distances between six F atoms of anion and C−H groups of cation that involve C(2), C(Ring), and C(N) atomic species. The results are shown in Figure 7. In (9, 9) CNT, the angle distributions inside the channel are almost the same as those in the bulk phase. The angles between F atoms and C(2)−H and C(Ring)−H groups are around 140°, and the angles between F atoms and C(N)−H group are around 70° (see Figure 7A). The distances of F···H are distributed from 2.0 to 2.5 Å, and the shortest distance of 2.0 Å occurs between F atoms and C(2)−H group (see Figure 7B). In (10, 10) CNT, the angles are also distributed around 140° between F atoms and C(2)−H and C(Ring)−H groups and are around 70° between F atoms and C(N)−H groups (see Figure 7C). The distances of F···H are also from 2.0 to 2.5 Å. Although the structures of the hydrogen bonds are very similar to those in (9, 9) CNT, the distribution probability ($P(\theta)$ and $P(r)$) is very different. These results indicate that when the size of the CNT is large enough, the anions could move above the imidazolium planes, and F atoms of anion can also form hydrogen bond with C(4) and C(5) on imidazolium-based ring, so the C(Ring)−H···F structure of the hydrogen bond is the dominant structure in (10, 10) CNT. Generally speaking, hydrogen bonding remains the dominant interaction between cations and anions, and the structure of the hydrogen bond does not change much when the IL enters into the channel of CNT from the bulk liquid.

4. Thermodynamics of Entering into the CNT

The spontaneous entrance of IL into the channel of CNT described above is driven by favorable free energy at a certain temperature. We computed the free energies of insertions for a single cation, a single anion, and an ion-pair from the bulk phase to the channels of CNTs at 500 K temperature and 1 atm pressure. For each of these three cases, we used the expanded ensemble (EE) method to compute the excess free energies $\Delta G1$ and $\Delta G2$ of the transfer of a solute molecule from a (ideal) gas phase into CNT and into a bulk IL, respectively. In the EE simulation, the CNT system contained a single CNT as described in section 2.1, with periodic hexagonal box boundaries set just outside the CNT, so that the only available place for the ions of IL was inside the CNT. The trial insertions and removals were performed into completely filled CNT (that is, the free energies of the last anion or cation entering the CNT were computed), and a total approximate time of 40 ns was used for these calculations. Considering the size and asymmetry of the ions, we choose 21 subensembles with 0.05 interval for the insertion parameter α for $[bmim]^+$ cation, as well for the ion-pair, and 11 subensembles with 0.1 interval for the smaller symmetric $[PF_6]^-$ anion. In case of the bulk phase computations, the insertion/deletion was made into IL composed of 64 ions pairs totally, in a periodic cubic box. Figure 8 shows an example of reasonably optimized η_m parameters, as well as the calculated free energies in the case of insertion of $[Bmim]^+$ cations and PF_6^- anions into the channel of (9, 9) CNT (to plot the balancing factors and the free energy in the same figure, the free energy is plotted as G/kT in Figure 8, for $T = 500$ K). The optimized balancing factors coincide almost perfectly with the free energies

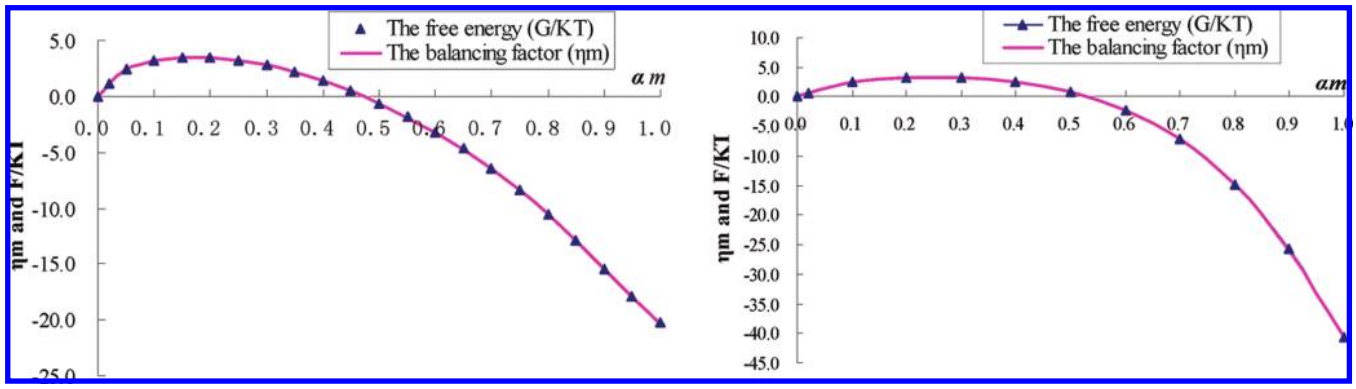

Figure 8. The changes of the balancing factor η_m and the free energy (plotted as G/kT, $T = 500$ K) with the number of subensembles α_m in (9, 9) CNT. (A) The distribution of $[bmim]^+$ cations in (9, 9) CNT. (B) The distribution of $[PF_6]^-$ anions in (9, 9) CNT.

TABLE 2: Calculated Free Energies from the EE Method

		free energy (kJ/mol)			
		[a]ΔG_1	[b]ΔG_2	[c]$RT \ln(V_2N_1/V_1N_2)$	[d]ΔG_3
(9, 9) CNT	cation	−84.37	−61.45	−4.34	−27.26
	anion	−169.33	−205.79	−4.34	32.12
	ion-pair	−255.82	−232.54	−4.34	−27.62
(10, 10) CNT	cation	−87.26	−61.45	−3.13	−29.34
	anion	−202.52	−205.79	−3.13	0.11
	ion-pair	−263.04	−232.54	−3.13	−33.18

[a] The excess free energies (kJ/mol) that a single cation, anion, or an ion-pair enter into the channel of the CNT from a gas phase. [b] The excess free energies (kJ/mol) that a single cation, anion, or an ion-pair enter into the bulk liquid phase from a gas phase. [c] The difference of ideal contributions to the Gibbs free energy in the CNT and the bulk liquid phase. [d] The Gibbs free energy change (kJ/mol) that a single cation, anion, or ion-pair enters into the channel of the CNT from the bulk liquid.

of the particle insertion. The dependence of the optimized parameters η_m on the insertion parameters α_m follows the pattern: first, a rapid growth of parameters η_m with the parameters α_m, corresponding to a positive free energy change to create a cavity in the solvent. Next, when the parameter α_m is approaching 1.0, the attractive part of interactions plays an important role, and optimized parameters η_m, as well as the free energies (G/KT), decrease, eventually becoming negative (see Figure 8). Similar patterns can also be obtained in (10, 10) CNT as well as in the bulk phase case.

We also calculated the vaporization enthalpy of a neutral ion-pair to test the reliability of EE method. The calculated vaporization enthalpy is 119.70 kJ/mol, which is very near to the experimental value of 115.0 kJ/mol.[15,53] The resulting excess free energies are shown in Table 2. Because the CNT and bulk calculations were made in different volumes and for different number of particles, the ideal gas contribution to the total Gibbs free energy, $G_{id} = RT \ln(N/V)$, should be taken into account while computing the difference of free energies between the bulk and the CNT phases. Thus, the free energy changes ($\Delta G3$) for a single cation, anion, and an ion-pair entering into the channel of the CNT from the bulk phase can be obtained through the following equation.

$$\Delta G3 = \Delta G1 - \Delta G2 + RT \ln\left(\frac{V_2 N_1}{V_1 N_2}\right) \qquad (4)$$

where N_1 is the number of ions of the inserted type in CNT, V_1 is the cell volume in CNT simulation, while N_2 and V_2 are the corresponding parameters for the bulk calculations.

From the data of Table 2, it can be seen that a single cation is favored by −27.3 kJ/mol free energy and can enter into the channel of the (9, 9) CNT from the bulk liquid phase. However, the free energy 32.1 kJ/mol for a single anion is high and positive, which makes it very difficult for the anion to enter into the channel of this CNT spontaneously. It is consistent with the previous conclusion of Figure 3 that the cation is always faster than the anion to enter into the channel for the same entering number. Analysis of data of Table 2 also shows that the excess free energy for the cation is lower in CNT as compared to the bulk phase, while for the anion we have the opposite relationship, which is that an anion prefers to be in the bulk phase. An ion-pair is favored by −27.6 kJ/mol free energy as the driving force, so it can enter into the channel spontaneously. Therefore, a more favorable way of understanding the insertion process may be that a cation "pulls" an anion to enter into the channel of the CNT from the bulk liquid phase together. This picture is similar to that when insertion of a neutral ion-pair into a bulk liquid from the volatile species at the lowest enthalpy of vaporization is more favorable as compared to the non-neutral ionic cluster.[54] So it is more favorable that an ion-pair enters into the channel of the CNT instead of a single ion. The same situation can be found in the larger diameter (10, 10) CNT from Table 2. Yet when the size of the CNT is larger, all of the free energies ($\Delta G3$) are lower than those in (9, 9) CNT; especially for an anion, the free energy becomes 0.11, and this means that entrance into the (10, 10) CNT is more favorable than (9, 9) CNT, so it is indicated that the entrance for ions can be determined by the diameter of CNT.

5. Conclusion

In summary, we performed MD simulations and provided direct structural evidence about the form of crystallite and the anomalous phase behavior for the [bmim][PF_6] ionic liquid when confined in single-wall CNTs. Although the entering number for cations and anions is equal when the CNT was saturated, cations are always faster to enter into the channel of CNT than anions in the whole filling process. In the radial direction, ions stack in the same cylindrical ionic sheets in which the imidazolium rings of cations are perpendicular to the lateral plane. In axial direction of (9, 9) CNT, as compared to arrangement in the bulk phase, cations and anions arrange alternately inside the channel with the same interval of 5 Å, and one-dimensional more ordered pulse-like ionic chain forms. However, in the larger (10, 10) CNT, anions move above imidazolium planes of the cations and form ion-pairs with cations, and these ion-pairs arrange alternately with interval of about 5 Å. Therefore, the pattern of ionic stacking and

distribution is determined by the sizes of the CNTs. The angles of C−H···F bonds between the F atoms of anions and C−H groups of cations are distributed around 140°, and the F···H distances are distributed between 2.0 and 2.5 Å, which is a typical hydrogen-bond feature. Therefore, the hydrogen bonds remain the dominant interactions between cations and anions when IL is confined in the channel of the CNTs. According to the free energies, determining the driving force for a single cation, anion, or an ion-pair to enter into the channel of CNT from the bulk phase, it is found that a cation can enter into the CNT, mostly due to favorable dispersion Lennard-Jones interactions (representing in fact the electronic attraction by CNT π-electrons), but it is very difficult for an anion to enter into the channel of the CNT spontaneously. A more favorable way can be described as an ion-pair entering, with a cation "pulling" an anion by hydrogen bonds to enter into the channel of the CNT together. The above results may give a clear structural and thermodynamic picture of the anomalous phase behavior of [bmim][PF_6], changing from liquid in the bulk to high melting point crystallite in CNTs. It can be predicted that other structurally similar ionic liquids, which are composed of the imidazolium-based cations, such as $[Amim]^+$ (A = methyl, ethyl, and propyl), or even pyridinium-based cations, $[N-bupy]^+$, and the anions, BF_4^-, $AlCl_4^-$, or NO_3^-, may show similar phase behavior and form the crystallite when confined inside the channels of the CNTs. The high melting points that these ionic liquids possess may be adjusted by confinement in different size CNTs.

Acknowledgment. This work was supported by the National Science Fund of China for Distinguished Young Scholar (20625618), the National Basic Research Program of China (973 Program, 2009CB219902), the National Natural Scientific Fund of China (20603040), and the Swedish Research Council (621-2007-5256).

References and Notes

(1) Welton, T. *Chem. Rev.* **1999**, *99*, 2071.
(2) Earle, M. J.; Seddon, K. R. *Pure Appl. Chem.* **2000**, *72*, 1391.
(3) Kanakubo, M.; Umecky, T.; Aizawa, T.; Kurata, Y. *Chem. Lett.* **2005**, *34*, 324.
(4) Hanke, C. G.; Price, S. L.; Lynden-Bell, R. M. *Mol. Phys.* **2001**, *99*, 801.
(5) Hanke, C. G.; Lynden-Bell, R. M. *J. Phys. Chem. B* **2003**, *107*, 10873.
(6) Del Popolo, M. G.; Voth, G. A. *J. Phys. Chem. B* **2004**, *108*, 1744.
(7) Yan, T.; Burnham, C. J.; Del Popolo, M. G.; Voth, G. A. *J. Phys. Chem. B* **2004**, *108*, 11877.
(8) Wang, Y.; Voth, G. A. *J. Am. Chem. Soc.* **2005**, *127*, 12192.
(9) Earle, M. J.; McCormac, P. B.; Seddon, K. R. *Green Chem.* **1999**, *1*, 23.
(10) Sheldon, R. *Chem. Commun.* **2001**, 2399.
(11) Dong, K.; Zhang, S. J.; Wang, D. X.; Yao, X. Q. *J. Phys. Chem. A* **2006**, *110*, 9775.
(12) Huang, X.; Margulis, C. J.; Li, Y.; Berne, B. J. *J. Am. Chem. Soc.* **2005**, *127*, 17842.
(13) Margulis, C. J. *Mol. Phys.* **2004**, *102*, 829.
(14) Margulis, C. J.; Stern, H. A.; Berne, B. *J. Phys. Chem. B* **2002**, *106*, 12017.
(15) Morrow, T. I.; Maginn, E. J. *J. Phys. Chem. B* **2002**, *106*, 12807.
(16) Liu, Y. D.; Zhang, Y.; Wu, G. Z.; Hu, J. *J. Am. Chem. Soc.* **2006**, *128*, 7456.
(17) Fukushima, T.; Kosaka, A.; Ishimura, Y.; Yamamoto, T.; Takigawa, T.; Ishii, N.; Aida, T. *Science* **2003**, *300*, 2072.
(18) Chen, S. M.; Wu, G. Z.; Sha, M. L.; Huang, S. R. *J. Am. Chem. Soc.* **2007**, *129*, 2416.
(19) Tasis, D.; Tagmatarchis, N.; Bianco, A.; Prato, M. *Chem. Rev.* **2006**, *106*, 1105.
(20) Cao, D. P.; Zhang, X. R.; Chen, J. F.; Wang, W. C.; Yun, J. *J. Phys. Chem. B* **2003**, *107*, 13286.
(21) Hinds, B. J.; Chopra, N.; Rantell, T.; Andrews, R.; Gavalas, V.; Bachas, L. G. *Science* **2004**, *303*, 5654.
(22) Kalra; Garde, S.; Hummer, G. *Proc. Natl. Acad. Sci. U.S.A.* **2003**, *100*, 10175.
(23) Kong, J.; Franklin, N. R.; Zhou, C. W.; Chapline, M. G.; Peng, S.; Cho, K. J.; Dai, H. J. *Science* **2000**, *287*, 5453.
(24) Liu, C.; Fan, Y.; Cong, H. T.; Cheng, H. M.; Dreselhaus, M. S. *Science* **1999**, *286*, 1127.
(25) Sazonova, V.; Yaish, Y.; Ustunel, H.; Roundy, D.; Arias, T. A.; Mceuen, P. L. *Nature* **2004**, *431*, 284.
(26) Snow, E. S.; Perkins, F. K.; Houser, E. J.; Badescu, S. C.; Reinecke, T. L. *Science* **2005**, *307*, 1942.
(27) Khlobystov, A. N.; Britz, D. A.; Briggs, G. A. D. *Acc. Chem. Res.* **2005**, *38*, 901.
(28) Hummer, G.; Rasaiah, J. C.; Noworyta, J. P. *Nature* **2001**, *414*, 188.
(29) Holt, J. K.; Park, H. Y.; Wang, Y. M.; Stadermann, M.; Artyuhin, A. B.; Grigoropoulos, C. P.; Noy, A.; Bakajin, O. *Science* **2006**, *312*, 1034.
(30) Wang, J.; Zhu, Y.; Zhou, J.; Lu, X. H. *Acta Chim. Sin.* **2003**, *61*, 1891.
(31) Bai, J.; Su, C. R.; Parra, R. D.; Zeng, X. C.; Tanaka, H.; Koga, K.; Li, J. M. *J. Chem. Phys.* **2003**, *118*, 3913.
(32) Byl, O.; Liu, J. C.; Wang, Y.; Yim, W.-L.; Johnson, J. K.; Yates, J. T. *J. Am. Chem. Soc.* **2006**, *128*, 12090.
(33) Koga, K.; Parra, R. D.; Tanaka, H.; Zeng, X. C. *J. Chem. Phys.* **2000**, *113*, 5037.
(34) Ajayan, P. M.; Ebbesen, T. W. *Rep. Prog. Phys.* **1997**, *60*, 1025.
(35) Wilson, M. *Nano Lett.* **2004**, *2*, 299.
(36) Wilson, M. *J. Chem. Phys.* **2006**, *124*, 124706.
(37) Wilson, M.; Friedrichs, S. *Acta Crystallogr., Sect. A* **2006**, *26*, 287.
(38) Wilson, M.; Madden, P. A. *J. Am. Chem. Soc.* **2001**, *123*, 2101.
(39) Huddleston, J. G.; Visser, A. E.; Reichert, W. M.; Willauer, H. D.; Broker, G. A.; Rogers, R. D. *Green Chem.* **2001**, *3*, 156.
(40) Fredlake, C. P.; Crosthwaite, J. M.; Hert, D. G.; Aki, S. N. V. K.; Brennecke, J. F. *J. Chem. Eng. Data* **2004**, *49*, 954.
(41) Martyna, G. J.; Tuckerman, M. E.; Tobias, D. J.; Klein, M. L. *Mol. Phys.* **1996**, *87*, 1117.
(42) Kalra, A.; Hummer, G.; Garde, S. *J. Phys. Chem. B* **2004**, *108*, 544.
(43) Liu, Z. P.; Huang, S. P.; Wang, W. C. *J. Phys. Chem. B* **2004**, *108*, 12978.
(44) Lyubartsev, A. P.; Laaksonen, A. *Comput. Phys. Commun.* **2000**, *128*, 565.
(45) Tuckerman, M.; Berne, B. J.; Martyna, G. J. *J. Chem. Phys.* **1992**, *97*, 1990.
(46) Lyubartsev, A. P.; Forrisdahl, O. K.; Laaksonen, A. *J. Chem. Phys.* **1998**, *108*, 227.
(47) Lyubartsev, A. P.; Laaksonen, A.; Vorontsov-Velyaminov, P. N. *Mol. Simul.* **1996**, *18*, 43.
(48) Lyubartsev, A. P.; Jacobsson, S. P.; Sundholm, G.; Laaksonen, A. *J. Phys. Chem. B* **2001**, *105*, 7775.
(49) Luder, K.; Kjellander, R. *J. Phys. Chem. B* **2006**, *110*, 15514.
(50) Koga, K.; Gao, G. T.; Tanaka, H.; Zeng, X. C. *Nature* **2001**, *412*, 802.
(51) Talaty, E. R.; Raja, S.; Storhaug, V. J.; Dölle, A.; Carper, W. R. *J. Phys. Chem. B* **2004**, *108*, 13177.
(52) Bondi, A. J. *J. Phys. Chem.* **1964**, *68*, 441.
(53) Shah, J.; Brennecke, J. F.; Maginn, E. J. *Green Chem.* **2002**, *4*, 112.
(54) Kelkar, M. S.; Maginn, E. J. *J. Phys. Chem. B* **2007**, *111*, 9492.

JP900533K